

One-dimensional spin-1/2 fermionic gases with two-body losses: Weak dissipation and spin conservation

Lorenzo Rosso¹, Davide Rossini^{2,3}, Alberto Biella^{1,4} and Leonardo Mazza^{1,*}

¹*LPTMS, Université Paris-Saclay, CNRS, 91405 Orsay, France*

²*Dipartimento di Fisica, Università di Pisa, Largo Pontecorvo 3, 56127 Pisa, Italy*

³*INFN, Sezione di Pisa, Largo Pontecorvo 3, 56127 Pisa, Italy*

⁴*INO-CNR BEC Center and Dipartimento di Fisica, Università di Trento, 38123 Povo, Italy*



(Received 16 April 2021; accepted 15 October 2021; published 8 November 2021)

We present a theoretical analysis of the dynamics of a one-dimensional spin-1/2 fermionic gas subject to weak two-body losses. Our approach highlights the crucial role played by spin conservation in the determination of the full time evolution. We focus in particular on the dynamics of a gas that is initially prepared in a Dicke state with a fully symmetric spin wave function, in a band insulator, or in a Mott insulator. In the latter case, we investigate the emergence of a steady symmetry-resolved purification of the gas. Our results could help with the modelization and understanding of recent experiments with alkaline-earth(-like) gases like ytterbium and fermionic molecules.

DOI: [10.1103/PhysRevA.104.053305](https://doi.org/10.1103/PhysRevA.104.053305)

I. INTRODUCTION

Experiments with ultracold gases are often regarded as paradigmatic studies of closed many-body quantum systems [1], yet they always suffer from the continuous leakage of particles into the vacuum chamber. In general, losses are responsible for decoherence and for the disappearance of quantum coherence [2]. Several studies have pointed out that they can also induce interesting effects: they can be used as a diagnostic tool for strong correlations [3–6], they can purify and cool the gas [7–10], and they can induce strong quantum correlations [11–15]. These effects are just a simple instance of the fact that in most situations the coupling to an environment, if properly engineered, can be beneficial and can be exploited for quantum technology purposes [16–20]. The correct theoretical modelization of the quantum dynamics induced by losses has thus emerged as an important problem and has recently attracted widespread attention [21–26].

Fermionic gases trapped in one-dimensional systems and subject to two-body losses feature a class of highly entangled stationary states with a fully symmetric Dicke-like spin wave function that could have important scientific and technological applications [27]. They have been the object of several experiments with molecular [28,29] and atomic gases [30], which, however, have not been able to certify the properties of the realized stationary state. Spin is conserved during the dissipative dynamics, and this is crucial for determining the steady properties. Various theoretical articles have addressed several aspects of the model and its dynamics [26,31], but the impact of spin conservation on the full dynamics, beyond determining its stationary properties, has not been understood yet.

In this article we present a simple theoretical framework for describing the lossy dynamics of a one-dimensional fermionic

gas with two-body losses that takes into account the exact conservation of spin. Even though most of the attention so far has focused on the strongly dissipative regime, we address here the weakly dissipative limit, which does not spoil the appearance of the highly entangled stationary states. We highlight the crucial role played by spin in causing a nontrivial relaxation dynamics that affects, in a qualitative way, the long-time behavior. The simplicity of the approach is a first step towards the modelization of experimental data, which could be obtained using alkaline-earth (e.g., strontium) or alkaline-earth-like (e.g., ytterbium [30]) atoms in the excited metastable state. We expect that our results may open the path to the realization of a consistent theory for the fermionic dynamics in the Zeno limit, which was recently done for bosons [24].

This article is organized as follows. In Sec. II we describe the setup. In Sec. III we derive a dynamical equation for the evolution of the particle density. Next, we compare our theoretical predictions with numerical simulations for three different classes of initial states: Dicke states with a fully symmetric spin wave function (Sec. IV), band insulators (Sec. V), and Mott insulators (Sec. VI). In Sec. VII we discuss the effect of weak interactions. Finally, in Sec. VIII we draw our conclusions.

II. THE SETUP

We consider a gas of spin-1/2 fermions trapped in a one-dimensional optical lattice with two-body contact interaction and two-body on-site losses. We introduce the fermionic operators $\hat{c}_{j,\sigma}^{(\dagger)}$, which satisfy canonical anticommutation relations, and the Hamiltonian of the Hubbard model, which describes the gas in the single-band approximation:

$$\hat{H} = -J \sum_j \sum_{\sigma=\uparrow,\downarrow} (\hat{c}_{j,\sigma}^\dagger \hat{c}_{j+1,\sigma} + \text{H.c.}) + U \sum_j \hat{n}_{j,\uparrow} \hat{n}_{j,\downarrow}. \quad (1)$$

*leonardo.mazza@universite-paris-saclay.fr

Here, J is the hopping amplitude, U is the interaction strength, and $\hat{n}_{j,\sigma} = \hat{c}_{j,\sigma}^\dagger \hat{c}_{j,\sigma}$ is the spin-resolved on-site lattice density operator.

The presence of local two-body losses is accounted for by the jump operators $\hat{L}_j = \sqrt{\gamma} \hat{c}_{j,\uparrow} \hat{c}_{j,\downarrow}$, where γ is the loss rate. The dynamics of the full density matrix $\rho(t)$ is described by a Lindblad master equation:

$$\dot{\rho}(t) = -\frac{i}{\hbar} [\hat{H}, \rho(t)] + \sum_j \hat{L}_j \rho(t) \hat{L}_j^\dagger - \frac{1}{2} \{ \hat{L}_j^\dagger \hat{L}_j, \rho(t) \}, \quad (2)$$

where $[\cdot, \cdot]$ denotes the commutator and $\{\cdot, \cdot\}$ denotes the anticommutator. In the experimental situations that we want to model [30], i.e., those in which losses are intrinsic, the ratio γ/U is determined by atomic (or molecular) properties and is of the order of unity; the ratio γ/J is instead tunable at will by modulating the strength of the optical lattice potential. We note that there are experiments in which the ratio γ/U can be tuned at will by means of, for instance, laser light, as was done in Ref. [32].

We introduce the operator associated with the total spin of the gas: $\hat{S} = \frac{\hbar}{2} \sum_{j,\sigma,\sigma'} \hat{c}_{j,\sigma}^\dagger \vec{\sigma}_{\sigma\sigma'} \hat{c}_{j,\sigma'}$, where $\vec{\sigma}_{\sigma\sigma'}$ is a vector whose components are the Pauli matrices. Since a two-body loss does not change the spin of the gas along any direction (the doubly occupied state has spin 0), the dynamics expressed by Eq. (2) is spin conserving, and the expectation value of the spin along any direction, $\vec{S} \cdot \vec{n}$, is a constant of motion. It follows that $\langle \hat{S}^2 \rangle$ is also a constant of motion. The main purpose of this article is to show how the presence of this constraint influences the dynamics.

III. POPULATION DYNAMICS FOR WEAK DISSIPATION

We focus on the simplest experimental observable, $\hat{N} = \sum_{j,\sigma} \hat{n}_{j,\sigma}$, and characterize how the number of fermions contained in the sample decreases in time because of loss processes. We will use the notation $\langle \hat{A} \rangle_t$ to denote the time-dependent expectation value of the observable \hat{A} , namely, $\langle \hat{A} \rangle_t \doteq \text{tr}[\rho(t)\hat{A}]$.

With simple algebraic passages, it is possible to show that $N(t) \doteq \langle \hat{N} \rangle_t$ obeys the following equation, which has an intuitive physical meaning:

$$\frac{d}{dt} N(t) = -2\gamma \left\langle \sum_j \hat{n}_{j,\uparrow} \hat{n}_{j,\downarrow} \right\rangle_t. \quad (3)$$

Since we cannot treat in an exact analytical way the right-hand side (rhs) of this equation, we perform a series of approxima-

$$\text{Var} N_t = \langle \hat{N}^2 \rangle_t - \langle \hat{N} \rangle_t^2, \quad \hat{\Pi} = \sum_k \hat{n}_{k,\uparrow} \hat{n}_{k,\downarrow},$$

$$\hat{T}_u = \sum_{\delta k \in [0, \frac{\pi}{2}]} (\hat{c}_{\frac{\pi}{2}+\delta k, \uparrow}^\dagger \hat{c}_{-\frac{\pi}{2}-\delta k, \uparrow} \hat{c}_{\frac{\pi}{2}-\delta k, \downarrow}^\dagger \hat{c}_{-\frac{\pi}{2}+\delta k, \downarrow} + \hat{c}_{\frac{\pi}{2}-\delta k, \uparrow}^\dagger \hat{c}_{-\frac{\pi}{2}-\delta k, \uparrow} \hat{c}_{\frac{\pi}{2}+\delta k, \downarrow}^\dagger \hat{c}_{-\frac{\pi}{2}+\delta k, \downarrow} + \text{H.c.}). \quad (7b)$$

Equation (6) is the main result of our study: it highlights the crucial interplay between the number of particles, its variance, the spin of the gas, and various correlators of the gas in momentum space. In particular, $\hat{\Pi}$ is a density-density correlator;

that are well justified in the limit of weak dissipation, $\hbar\gamma \ll J$. Note that this is also the limit of weak interactions, $U \ll J$, and the first approximation that we perform, discussed extensively in Sec. VII, consists of completely neglecting interactions.

Using semiclassical reasoning, we observe that in the limit $\hbar\gamma \ll J$, losses act on timescales that are much longer than those characterizing the unitary time evolution. In between two loss processes, the long unitary dynamics acts and averages out any time-dependent physical operator or correlator. We thus employ a *time-dependent stationarity condition* and assume that the system is always in a stationary state of the Hamiltonian and that particle losses are responsible for a dynamics that explores this subspace of the state space. This theoretical approach follows from several ideas put forward in the context of weakly dissipative systems [33,34], which have been largely employed in recent theoretical studies of lossy systems [23,24].

In practice, we focus on the operator that is responsible for losses, $\langle \sum_j \hat{n}_{j,\uparrow} \hat{n}_{j,\downarrow} \rangle_t$, and expand it in the basis of plane waves, $\hat{c}_{k,\sigma} = L^{-\frac{1}{2}} \sum_j e^{-ikj} \hat{c}_{j,\sigma}$, which are the eigenmodes of the free-fermion Hamiltonian dynamics, obtaining

$$\frac{1}{L} \sum_{k,q,w,z} \sum_n \delta_{k+q-w-z, 2\pi n} \langle \hat{c}_{k,\uparrow}^\dagger \hat{c}_{w,\uparrow} \hat{c}_{q,\downarrow}^\dagger \hat{c}_{z,\downarrow} \rangle_t. \quad (4)$$

The Kronecker δ ensures that only momentum-conserving correlators (modulus 2π) are considered. The Hamiltonian time evolution of the correlators in (4) is easily written:

$$\langle \hat{c}_{k,\uparrow}^\dagger \hat{c}_{w,\uparrow} \hat{c}_{q,\downarrow}^\dagger \hat{c}_{z,\downarrow} \rangle_t = e^{-\frac{i}{\hbar}(E_k+E_q-E_w-E_z)t} \langle \hat{c}_{k,\uparrow}^\dagger \hat{c}_{w,\uparrow} \hat{c}_{q,\downarrow}^\dagger \hat{c}_{z,\downarrow} \rangle_0, \quad (5)$$

where $E_k = -2J \cos(k)$ is the energy eigenvalue associated with the k th mode of the free-fermion Hamiltonian. The request for the system to explore only stationary states requires us to keep only the energy-conserving correlators because their expectation value does not depend on time.

This leads to an expression that can be further simplified by taking into account the conserved quantity \hat{S}^2 (see Appendix A for the explicit calculations):

$$\dot{N}(t) = -\frac{2\gamma}{L} \left[\frac{N(t)^2}{4} + \frac{N(t)}{2} + \frac{\text{Var} N_t}{4} - \frac{\langle \hat{S}^2 \rangle_0}{\hbar^2} - \langle \hat{\Pi} \rangle_t + \langle \hat{\Sigma}_{\frac{\pi}{2}} \rangle_t + \langle \hat{T}_u \rangle_t \right], \quad (6)$$

with

$$\hat{\Sigma}_{\frac{\pi}{2}} = \sum_{k \neq q, k \neq \pi - q} \hat{c}_{k,\uparrow}^\dagger \hat{c}_{q,\uparrow} \hat{c}_{\pi-k,\downarrow}^\dagger \hat{c}_{\pi-q,\downarrow}, \quad (7a)$$

$\hat{\Sigma}_{\frac{\pi}{2}}$ takes into account correlators that are symmetric with respect to the center of the band, located at $k = \pm\pi/2$ (note that in this operator momenta are defined mod 2π to restrict them to the first Brillouin zone); and \hat{T}_u considers umklapp

terms, where the difference in momenta is equal to $\pm 2\pi$. The presence of the two latter operators is a lattice effect: the symmetry of the band with respect to $k = \pm\pi/2$ is not present for a quadratic band in the continuum limit, where $E_k \propto k^2$; similarly, umklapp processes exist only in discrete systems.

A. The thermodynamic limit

The terms which appear on the rhs of Eq. (6) have different scalings in the thermodynamic limit. We divide both the rhs and left-hand side of Eq. (6) by L and focus on intensive quantities, whose limit is finite in the thermodynamic limit, which we simply indicate as $\lim_{L \rightarrow \infty}$. We define the lattice density $n(t) = \lim_{L \rightarrow \infty} N(t)/L$, the lattice spin density $s_0^2 = \lim_{L \rightarrow \infty} \langle \hat{S}^2 \rangle_0 / L^2$, and the correlator $\sigma_{\frac{\pi}{2}}(t) = \lim_{L \rightarrow \infty} \langle \hat{\Sigma}_{\frac{\pi}{2}} \rangle_t / L^2$. It is expected that $\text{Var}N_t$ and $N(t)$ scale to zero once divided by L^2 ; a similar result is expected for $\langle \hat{\Pi} \rangle$ and $\langle \hat{T}_u \rangle$ because they are the sum of L terms. We obtain the simpler equation

$$\dot{n}(t) = -2\gamma \left[\frac{n(t)^2}{4} - \frac{s_0^2}{\hbar^2} + \sigma_{\frac{\pi}{2}}(t) \right]. \quad (8)$$

Note that a finite spin $\langle \hat{S}^2 \rangle_0 \neq 0$ could have zero value $s_0 = 0$ in the thermodynamic limit.

We now propose an argument demonstrating that $\sigma_{\frac{\pi}{2}}(t) = 0$ using the fact that the local properties of the system in the thermodynamic limit can be discussed also within the framework of the time-dependent generalized Gibbs ensemble (GGE) [24,33]. This is a stronger approximation with respect to that used at the beginning of this section to derive Eq. (6) and requires that the system is not only always in a stationary state of the Hamiltonian but also in the specific class of states that are GGE. These states describe the local properties of systems in the thermodynamic limit after a long unitary time evolution. In the case of noninteracting fermions, a GGE is a Gaussian state that is factorized in momentum space. We present a detailed derivation in Appendix B and report here the result:

$$\dot{N}(t) = -\frac{2\gamma}{L} \left[\frac{N(t)^2}{4} - \frac{\langle \hat{S}_x \rangle^2 + \langle \hat{S}_y \rangle^2 + \langle \hat{S}_z \rangle^2}{\hbar^2} \right]. \quad (9)$$

If we focus on intensive quantities and address the thermodynamic limit, we observe that

$$\lim_{L \rightarrow \infty} \frac{\langle \hat{S}^2 \rangle}{L^2} = \lim_{L \rightarrow \infty} \frac{\langle \hat{S}_x \rangle^2 + \langle \hat{S}_y \rangle^2 + \langle \hat{S}_z \rangle^2}{L^2}, \quad (10)$$

with their difference $\sum_i \langle \hat{S}_i^2 \rangle - \langle \hat{S}_i \rangle^2$ being only $\sum_i \text{Var}S_i$, which is subleading. We obtain the equation

$$\dot{n}(t) = -2\gamma \left[\frac{n(t)^2}{4} - \frac{s_0^2}{\hbar^2} \right]. \quad (11)$$

By employing this GGE approximation we thus see that $\sigma_{\frac{\pi}{2}} = 0$, and that can be neglected. Moreover, this discussion has the advantage of showing explicitly that Eq. (11) does not take into account exactly the spin conservation.

Equation (6) is thus a more refined version of Eq. (11) because it includes finite-size corrections. Whereas this might seem an unnecessary overshooting, testing this theory with numerical tools is demanding, and we present state-of-the-art

numerical simulations for lattices up to $L = 10$. For these lattice lengths, in several cases the dynamics predicted by Eq. (11) is recognizable only at short times. This higher accuracy comes at the price of introducing several new variables, for which we have not been able to write satisfactory and simple dynamical equations; when necessary, we will show how to treat them.

B. Continuum limit

The study presented so far can be easily extended to a setup without the optical lattice of length L (see also Ref. [27]). Introducing the fermionic fields $\hat{\Psi}_\sigma(x)$ (with $\sigma = \uparrow, \downarrow$), the atomic mass m , and the interaction parameter g , the Hamiltonian reads

$$\hat{H}_c = \int \sum_\sigma \hat{\Psi}_\sigma^\dagger(x) \left(-\frac{\hbar^2}{2m} \partial_x^2 \right) \hat{\Psi}_\sigma(x) dx + g \int \hat{\Psi}_\uparrow^\dagger(x) \hat{\Psi}_\uparrow(x) \hat{\Psi}_\downarrow^\dagger(x) \hat{\Psi}_\downarrow(x) dx. \quad (12)$$

In order to include loss processes we introduce the jump operators $\hat{J}(x) = \sqrt{\xi} \hat{\Psi}_\uparrow(x) \hat{\Psi}_\downarrow(x)$, where ξ is the rate associated with two-body losses. The full Lindblad dynamics reads

$$\dot{\rho}(t) = -\frac{i}{\hbar} [\hat{H}_c, \rho(t)] + \int \hat{J}(x) \rho(t) \hat{J}(x)^\dagger - \frac{1}{2} \{ \hat{J}(x)^\dagger \hat{J}(x), \rho(t) \} dx. \quad (13)$$

We now focus on the weakly dissipative limit, characterized by a loss rate that is subleading with respect to the kinetic energy: $\xi \ll \hbar n/m$, where n is the gas density. Note that this inequality cannot be satisfied at all times for a gas that completely loses its population; however, as we will see, the problem that we are studying is characterized, in certain regimes, by a finite steady density.

With calculations similar to those presented above, one obtains the following dynamical equation for the population $N(t) = \langle \int \sum_\sigma \hat{\Psi}_\sigma^\dagger(x) \hat{\Psi}_\sigma(x) dx \rangle_t$ in the weakly dissipative limit:

$$\dot{N}(t) = -\frac{2\xi}{L} \left[\frac{N(t)^2}{4} + \frac{N(t)}{2} + \frac{\text{Var}N_t}{4} - \frac{\langle \hat{S}^2 \rangle_0}{\hbar^2} - \langle \hat{\Pi} \rangle_t \right]. \quad (14)$$

The above equation is identical to Eq. (6), where γ has been replaced with ξ . The definitions of the total spin \hat{S}^2 and of the $\hat{\Pi}$ observables are trivial generalizations of those presented above for a lattice. Operators $\hat{\Sigma}_{\frac{\pi}{2}}$ and \hat{T}_u instead do not appear because, as we have already seen, they are a lattice effect. In the rest of the article we will focus on only the lattice problem, and several results can be easily generalized to the continuum case.

IV. DICKE STATES AND STATIONARY POPULATIONS

The first test for the population equation (6) consists of its application to states whose spin part is fully symmetric like in a Dicke state, which are characterized by a spin quantum number $S = N/2$. It was pointed out in Ref. [27] that Dicke states (from now on we use this brief term to indicate any state

with $S = N/2$) are dark states of the dissipative dynamics: since spin is conserved and the minimal number of fermions that are necessary to create a spin- s state is $2s$, no particle can be lost from a Dicke state without changing the spin quantum number; that is, the loss cannot take place.

Equation (6) predicts that the population of Dicke states does not evolve in time. In order to prove this, we introduce the notation $|D_N\rangle$ for a generic Dicke state with N particles and spin $S = N/2$; the orbital part of the wave function can be arbitrary, provided it is fully antisymmetric. We show in Appendix C that for a generic linear superposition of Dicke states, $|\Psi_D\rangle = \sum_N c_N |D_N\rangle$, the following properties hold:

$$\langle \Psi_D | \hat{S}^2 | \Psi_D \rangle = \frac{\hbar^2}{2} \left(\frac{N^2 + \text{Var}N}{2} + N \right), \quad (15a)$$

$$\langle \Psi_D | \hat{\Pi} | \Psi_D \rangle = 0, \quad \langle \Psi_D | \hat{\Sigma}_{\frac{\pi}{2}} | \Psi_D \rangle = 0, \quad \langle \Psi_D | \hat{T}_u | \Psi_D \rangle = 0. \quad (15b)$$

From these properties we can deduce that Dicke states are stationary states of the dynamics: $\dot{N}(t) = 0$.

Equation (11) takes into account the spin conservation in the thermodynamic limit and predicts a stationary density

$$n_\infty = \frac{2}{\hbar} s_0. \quad (16)$$

Dicke states satisfy this relation; indeed, from the above formulas we obtain

$$\begin{aligned} \frac{s_0^2}{\hbar^2} &= \lim_{L \rightarrow \infty} \frac{\langle \Psi_D | \hat{S}^2 | \Psi_D \rangle}{\hbar^2 L^2} \\ &= \lim_{L \rightarrow \infty} \left(\frac{N^2 + \text{Var}N + 2N}{4L^2} \right) = \frac{n^2}{4}. \end{aligned} \quad (17)$$

V. DYNAMICS FROM A BAND INSULATOR

We now discuss the dissipative dynamics starting from a band insulator, $|\Psi_{\text{BI}}\rangle = \prod_j \hat{c}_{j,\uparrow}^\dagger \hat{c}_{j,\downarrow}^\dagger |0\rangle$, where any lattice site is doubly occupied and the initial population is $2L$. The system is in a spin-0 state, $\langle \hat{S}^2 \rangle = 0$, and a simple calculation shows that $\langle \hat{\Pi} \rangle_0 = L$, $\langle \hat{\Sigma}_{\frac{\pi}{2}} \rangle_0 = 0$, and $\langle \hat{T}_u \rangle_0 = 0$. The prediction for the dynamics of the lattice density $n(t)$ in the thermodynamic limit is easily obtained from Eq. (11):

$$n(t) = \frac{2}{1 + \gamma t}. \quad (18)$$

The full solution of Eq. (6) is more challenging because it is not obvious how to give a prediction for the time dependence of $\text{Var}N_t$, $\langle \hat{\Pi} \rangle_t$, $\langle \hat{\Sigma}_{\frac{\pi}{2}} \rangle_t$, and $\langle \hat{T}_u \rangle_t$ (we could not derive closed expressions for their time derivatives, and a Gaussian expansion gives wrong predictions, possibly because here we are looking for beyond-Gaussian effects).

We can use Eq. (6) to get insights into the long-time dynamics of a finite system since when $N(t)$ tends to zero, we have $N(t)^2 \ll N(t)$. In this limit it is possible to model the number of particles as a Bernoullian distribution, where with probability p the system has two particles and with probability $1 - p$ it is empty. For such a distribution, $N = 2p$, $\text{Var}N \sim 4p$, and thus, we estimate that, in the long-time limit, $\text{Var}N_t \sim 2N(t)$. Concerning $\langle \hat{\Pi} \rangle$, we can bound it in the following way: since $\hat{\Pi}$ is a non-negative operator, $\langle \hat{\Pi} \rangle \geq 0$; since $\hat{n}_{k,\uparrow} \hat{n}_{k,\downarrow} \leq$

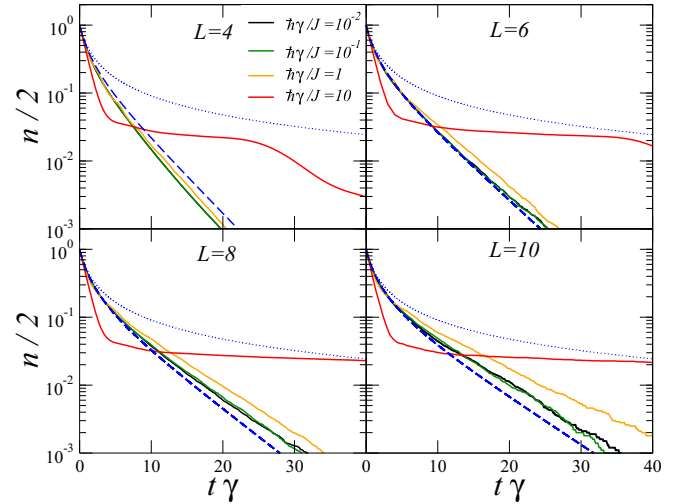


FIG. 1. Dissipative dynamics of the normalized density of a band insulator for $L = 4, 6, 8,$ and 10 . The various colors refer to different dissipation strengths, from $\hbar\gamma/J = 10^{-2}$ to $\hbar\gamma/J = 10$ (see legend). The thin blue dotted curve is the prediction for the thermodynamic limit in Eq. (18), whereas the thick blue dashed curve is Eq. (20). The latter faithfully describes the weakly dissipative limit even at small sizes. The plot highlights the collapse of the curves for $\hbar\gamma/J = 10^{-2}, 10^{-1},$ and 1 . On the other hand, the appearance of a different behavior in the strongly dissipative Zeno limit is evident.

$\hat{n}_k/2$, we can write $\langle \hat{\Pi} \rangle < N/2$. If we neglect the contributions from $\hat{\Sigma}_{\frac{\pi}{2}}$ and \hat{T}_u (which is justified *a posteriori* by numerical simulations), we thus obtain that the long-time scaling is exponential: $N(t) \sim \exp(-t/\tau)$, with $L/(2\gamma) < \tau < L/\gamma$. In all cases, τ depends on the size, which is compatible with the fact that in the thermodynamic limit we expect an algebraic decay.

We verified these predictions with exact numerical simulations of the full master equation using the stochastic quantum trajectory approach [35] (for $L > 4$); we have used the PYTHON-based QUTIP package [36,37], which allowed us to push our analysis up to $L = 10$ sites with high statistics ($N_{\text{traj}} \geq 10^3$, with N_{traj} being the number of trajectories); when they are not specified, we are using open boundary conditions. The results of our numerical simulations (always with open boundary conditions) are shown in Fig. 1, where we consider four values of $\hbar\gamma/J$, ranging from 10^{-2} to 10 . Note that here and in the subsequent figures we omitted the error bars since the statistical errors associated with the averaging over the trajectories remain negligible on the scales of the various plots, up to densities $n \lesssim 10^{-2}$. For $\hbar\gamma/J \leq 1$ we observe a universal behavior even at small sizes. Data are affected by important finite-size effects, and indeed, no collapse of curves at different L has been observed (see Appendix D). The comparison with the prediction in (18), which is plotted as a thin blue dotted line, is satisfactory only at short times, and it improves for increasing lattice size. For $L = 10$ there is a quantitative agreement until the density decreases to $n \sim 0.4$. For longer times, we observe the appearance of an exponential decay, as predicted in the previous paragraph.

We use our numerical simulations to link $\text{Var}N_t$ and $\langle \hat{\Pi} \rangle_t$ to $N(t)$; motivated by the data shown in Appendix D,

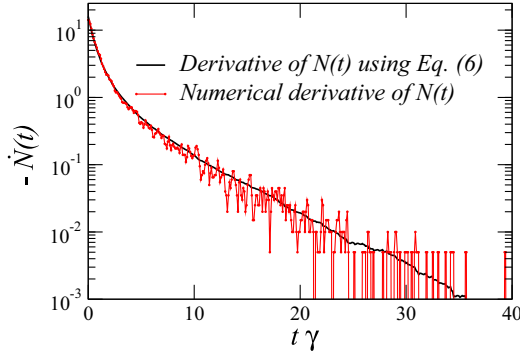


FIG. 2. Time derivative of the population $\dot{N}(t)$ for $L = 8$ and $\hbar\gamma/J = 10^{-1}$. Thick black solid line: calculation of $\dot{N}(t)$ using the right-hand side of Eq. (6) by running a numerical simulation with $N_{\text{traj}} = 2000$ quantum trajectories that computes explicitly all the necessary quantities. Thin red line: numerical derivative of $N(t)$ computed with $N_{\text{traj}} = 2000$ quantum trajectories and using the Euler method.

we propose

$$\langle \hat{\Pi} \rangle_t \simeq \frac{N(t)}{L} + \frac{L - 2N(t)^2}{4L^2}, \quad (19a)$$

$$\begin{aligned} \text{Var}N_t &\simeq 2[N(t) - 2\langle \hat{\Pi} \rangle_t] \\ &\simeq \left(1 - \frac{2}{L}\right) \left(2N(t) - \frac{N(t)^2}{L}\right). \end{aligned} \quad (19b)$$

On the other hand, $\langle \hat{\Sigma}_{\frac{\pi}{2}} \rangle_t$ and $\langle \hat{T}_u \rangle_t$ are negligible at all times. We substitute these expressions into Eq. (6) and obtain the following solution:

$$n(t) = \frac{4\left(1 - \frac{2}{L}\right)}{L\{\exp\left[\left(1 - \frac{2}{L}\right)\frac{2\gamma t}{L}\right] - 1\} + 2 - \frac{4}{L}}. \quad (20)$$

The above equation is the theoretical prediction plotted in Fig. 1 as a thick blue dashed line, which provides a satisfactory description of our numerics.

Since this latter result has been obtained using the numerical data, we perform a direct investigation of whether Eq. (6) is a good tool for describing the population dynamics. We compute the numerical derivative of the data displayed in Fig. 1 for $L = 8$ and $\hbar\gamma/J = 0.1$ using Euler's method, and we compare the obtained curve with the prediction given by the rhs of Eq. (6) by running a numerical simulation that computes explicitly all the necessary quantities. The comparison is shown in Fig. 2, and the agreement is excellent, showing that Eq. (6) models the system even at small sizes. This confirms the general validity of the approximations employed to derive Eq. (6).

A. Periodic boundary conditions vs open boundary conditions

The numerical analysis of the dissipative dynamics of an initial band insulator shows that for periodic boundary conditions the stationary value of the population is not zero (see Fig. 3, top left panel). This result is in contrast to the expectation that Dicke states are unique stationary states: since $\langle \hat{S}^2 \rangle_0 = 0$, if this were the case, the stationary population

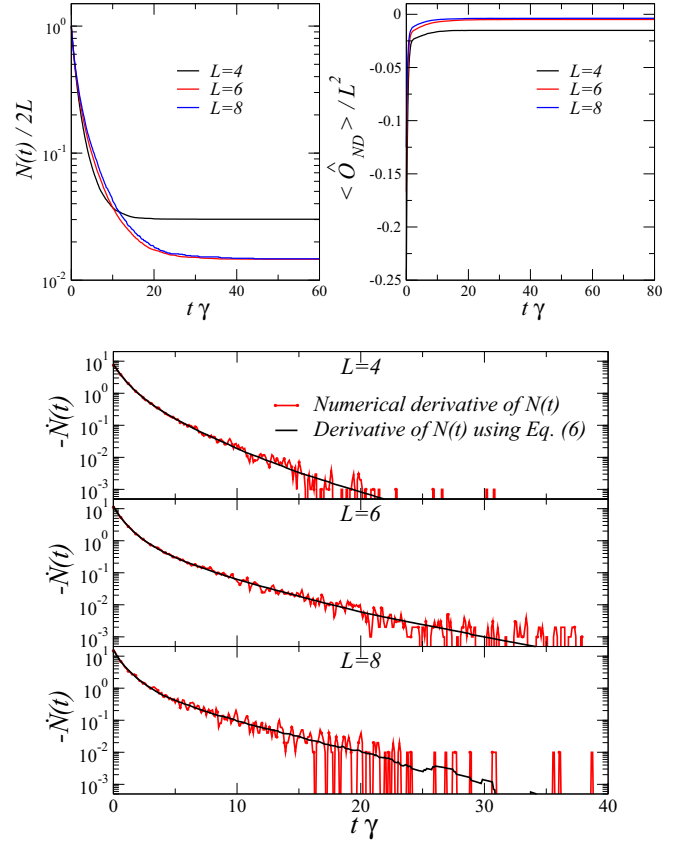


FIG. 3. Lossy dynamics from an initial band insulator with periodic boundary conditions using quantum trajectories ($N_{\text{traj}} = 10^4$ for $L = 4, 6$ and $N_{\text{traj}} = 10^3$ for $L = 8$) and $\hbar\gamma/J = 0.1$. Top left: dynamics of the population $N(t)$. Top right: at finite size, the stationary state is not Dicke, as quantified by the operator \hat{O}_{ND} . Bottom: time derivative of the population computed using the right-hand side of Eq. (6) and with the numerical derivative of $N(t)$.

would be zero, regardless of the boundary conditions. This problem was also mentioned in Ref. [27].

By looking at Eq. (6), we observe that a stationary state that is not a Dicke state is characterized by a nonzero expectation value of the operator $\hat{O}_{\text{ND}} = -\hat{\Pi} + \hat{\Sigma}_{\frac{\pi}{2}} + \hat{T}_u$; roughly speaking, $\langle \hat{O}_{\text{ND}} \rangle_{\text{ss}}$ measures the *non-Dickeness* of a stationary state. Whereas our numerics for open boundary conditions shows that $\langle \hat{O}_{\text{ND}} \rangle_t \sim \langle \hat{\Pi} \rangle_t$ and that $\langle \hat{\Pi} \rangle_{\text{ss}} \sim 0$, this is not true for periodic boundary conditions. In the top right panel of Fig. 3, we show that in the latter case the stationary value of $\langle \hat{O}_{\text{ND}} \rangle_{\text{ss}}$ is different from zero at finite size. This explains why the stationary state is not empty: it is not a Dicke state.

Yet if we consider $\langle \hat{O}_{\text{ND}} \rangle_{\text{ss}}/L^2$ in order to discuss the properties of the thermodynamic limit, such a value should tend to zero for $L \rightarrow \infty$. We have verified this scaling numerically for $\langle \hat{\Sigma}_{\frac{\pi}{2}} \rangle_{\text{ss}}$ and $\langle \hat{T}_u \rangle_{\text{ss}}$ (not shown). Remarkably, for some values of L the value of $\langle \hat{\Pi} \rangle_{\text{ss}}$ is zero, and for other ones it is not. This absence of a smooth dependence on L prevents us from seeing a clear tendency towards zero for $L \rightarrow \infty$ in the plots of $N(t \rightarrow \infty)/L$ and $\langle \hat{O}_{\text{ND}} \rangle_{\text{ss}}/L^2$ reported in Fig. 3. Nonetheless, from mathematical arguments we know that $\langle \hat{\Pi} \rangle_{\text{ss}}/L^2 \rightarrow 0$ for $L \rightarrow \infty$ because $\hat{\Pi}$ is the sum of L non-negative and bounded operators. This is sufficient to let us conclude that in

the thermodynamic limit $\langle \hat{O}_{ND} \rangle_{ss} \rightarrow 0$ and that the stationary state is Dicke and empty.

We conclude this section with two final messages. First, Eq. (11) retains its validity even with periodic boundary conditions when numerical simulations show finite-size effects that qualitatively deviate from the assumption that Dicke states are the only stationary states. Second, even in these situations, at finite size, Eq. (6) can be employed to describe the dynamics and to characterize deviations from stationary Dicke states. In order to support the latter statement, in the bottom panel of Fig. 3, we compare the time derivatives of the population computed from the numerical value of $N(t)$ and from Eq. (6), which display excellent agreement.

VI. DYNAMICS FROM A MOTT INSULATOR

A. Thermodynamic limit

We now consider an initial state with one particle per site, that is, a Mott insulator in the atomic limit.

Because of the spin, the manifold of such states spans a subspace of dimension 2^L . Conservation of spin during the dynamics takes here a nontrivial form because the spin of the gas can range from 0 to $L/2$. We can easily discuss the dynamics in the thermodynamic limit: the asymptotic number of particles is $n_\infty = \frac{2}{\hbar} s_0$, and the dynamics is given by

$$n(t) = n_\infty \tanh \left[\frac{n_\infty \gamma}{2} t + \operatorname{arctanh} \left(\frac{1}{n_\infty} \right) \right]. \quad (21)$$

This result displays in a clear way the interplay between spin conservation and dissipative dynamics. Not only are the stationary properties of the gas determined by the initial spin of the gas; the dynamics is also determined by it since stationary properties are approached with a typical decay time,

$$\tau = \frac{2}{\gamma n_\infty} = \frac{\hbar}{\gamma s_0}, \quad (22)$$

that depends on spin and that is shorter for larger spin values.

The link between the stationary number of particles and the typical decay time was already highlighted in Ref. [30], although the authors did not mention its connection to spin.

B. Finite-size effects

If we consider a Mott insulator with $N = L$ particles initialized in an eigenstate of \hat{S}^2 with quantum number S , the asymptotic number of particles can be exactly characterized for any size assuming that the final state is a Dicke state. In this case we expect that the stationary state has a well-defined number of particles given by the relation $N_\infty = 2S$.

When the initial Mott insulator is not an eigenstate of \hat{S}^2 , we expect the final state to be a linear superposition of Dicke states with different number of particles ($\operatorname{Var}N > 0$) and spin. Assuming stationarity, $\dot{N} = 0$, and recalling that for a linear superposition of Dicke states $\langle \hat{\Pi} \rangle = 0$, we obtain

$$N_\infty \leq \sqrt{\frac{4\langle \hat{S}^2 \rangle}{\hbar^2} + 1} - 1. \quad (23)$$

It is simple to verify that the bound is saturated when the initial state is an eigenstate of \hat{S}^2 .

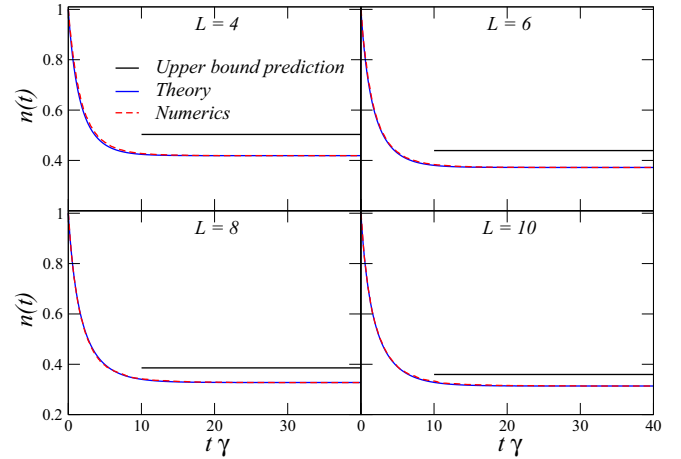


FIG. 4. Dissipative dynamics of a Néel state for $L = 4, 6, 8,$ and 10 for $\hbar\gamma/J = 0.1$. The time-dependent population is plotted as a red dashed line. The upper bound to the total population given in Eq. (23). The blue solid curve (theory) is a fit to the dynamics using Eq. (21) and taking n_∞ as the only fitting parameter.

C. Typical decay time and spin

In order to test these predictions we performed several numerical simulations of the full master equation for an initial Mott insulator. We consider as the initial state a Néel state with alternating spin up and down: $|\uparrow \downarrow \uparrow \downarrow \dots\rangle$. Results for the decaying populations are shown in Fig. 4. We observe that, since the initial state is not an eigenstate of \hat{S}^2 , the bound of Eq. (23) is satisfied but not saturated. It is shown that in this situation Eq. (21) provides an excellent description of the dynamics taking only n_∞ as the fit parameter. We have verified that the fitted value of n_∞ does not satisfy the relation with the spin, i.e., $n_\infty \neq \frac{2\sqrt{\langle \hat{S}^2 \rangle}}{\hbar L}$.

We further investigate the typical timescale with which the asymptotic number of particles is approached. The results in Fig. 5 show a clear exponential approach to the stationary value. We have investigated whether the analytical formulas given in Eq. (22) can give a quantitative prediction to the typical decay time τ . As shown in the plot, the formula

$$\tau = \frac{\hbar L}{\gamma \sqrt{\langle \hat{S}^2 \rangle}} \quad (24)$$

gives a remarkably good description of the numerical data. Less accurate results are instead obtained with the formula $\tau = 2/(\gamma n_\infty)$, where n_∞ has been taken from the previous fit; the discrepancy is solely ascribed to finite-size effects and is expected to disappear in the thermodynamic limit.

We finally perform a set of numerical simulations to test whether this latter relation between the decay time and the spin is true in general. We consider as the initial state an uncorrelated Mott insulator in which, on each lattice site, the spin \vec{S}_i is randomly oriented. In order to construct such a state, we randomly draw two angles, θ_i and ϕ_i , which identify a generic direction on the Bloch sphere, for every lattice site i . The goal of this procedure is not to sample in a uniform way the set of uncorrelated Mott insulators, but to generate states with widely variable values of $\langle \hat{S}^2 \rangle$. We have evolved

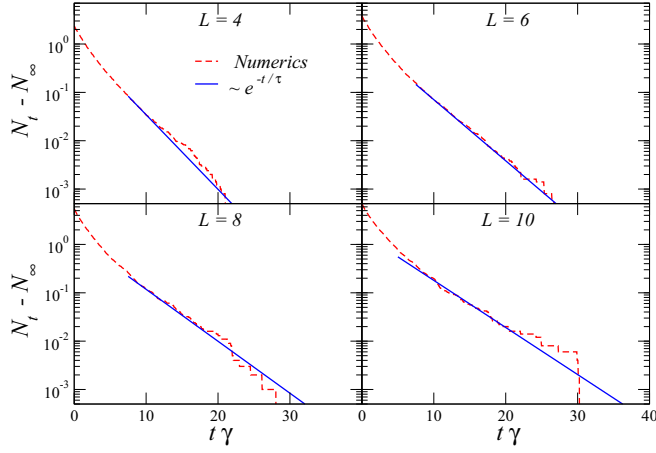


FIG. 5. Dissipative dynamics of a Néel state for $L = 4, 6, 8,$ and 10 for $\hbar\gamma/J = 0.1$ and long-time decay of $N(t)$ to the stationary value N_∞ . In all cases we observe an exponential decay. The blue solid curve is not a fit, but the decay obtained from the theoretical prediction $N_t - N_\infty = e^{-t/\tau}$ with τ given by Eq. (24), which provides an excellent description of the decay time at all lattice lengths.

in time 14 Mott insulators with uncorrelated and random site-dependent spin alignment; in all cases we observe an exponential approach to the stationary value of the number of particles.

We fit the typical timescale with which the asymptotic value is approached and compare it to the theoretical prediction given by Eq. (24). We first take as N_∞ the numerical value of the population at the longest computed time; we then fit $N(t) - N_\infty$ at intermediate times because at long times its value is comparable to the statistical error bars due to our stochastic sampling with quantum trajectories. The results shown in Fig. 6 display a clear correlation between the typical decay time predicted by the theory and the fitted one.

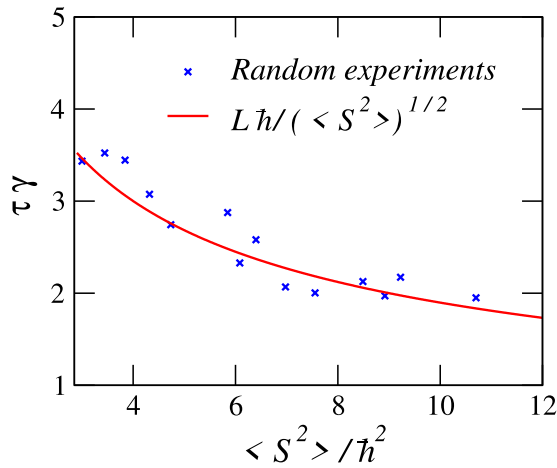


FIG. 6. Decay time of the population $N(t)$ approaching the asymptotic number of particles N_∞ as a function of $\langle S^2 \rangle / \hbar^2$ for $L = 6$ and $\hbar\gamma/J = 0.1$. Red solid line: theoretical curve for τ predicted in the thermodynamic limit (24). Blue crosses: numerical fits of the decay time τ performed for 14 random Mott insulators with 10^4 quantum trajectories.

Notice that the theoretical prediction has been derived in the thermodynamic limit, whereas here, we consider numerical simulations for $L = 6$.

D. Symmetry-resolved purity

When starting from a Mott insulator, the system features a nontrivial dynamics also in terms of the purity of the total density matrix:

$$\mathcal{P}_{\text{tot}} = \text{tr}[\rho(t)^2]. \quad (25)$$

Since the density matrix is reconstructed via the independent dynamics of N_{traj} quantum trajectories [35], we have

$$\rho(t) = \frac{1}{N_{\text{traj}}} \sum_{i=1}^{N_{\text{traj}}} |\psi_i(t)\rangle\langle\psi_i(t)|, \quad (26)$$

where $|\psi_i(t)\rangle$ is the i th trajectory at time t . Thus, combining Eq. (26) with Eq. (25), we get (from now on we will omit the time dependence)

$$\begin{aligned} \mathcal{P}_{\text{tot}} &= \frac{1}{N_{\text{traj}}^2} \sum_s \sum_{i,j=1}^{N_{\text{traj}}} \langle s|\psi_i\rangle\langle\psi_j|\psi_j\rangle\langle\psi_j|s\rangle \\ &= \frac{1}{N_{\text{traj}}^2} \sum_{i,j=1}^{N_{\text{traj}}} |\langle\psi_i|\psi_j\rangle|^2, \end{aligned} \quad (27)$$

where $\{|s\rangle\}$ is an orthonormal basis of the Hilbert space and in the second line we used $\sum_s |s\rangle\langle s| = \mathbb{I}$.

The dynamics of a single quantum trajectory is governed by an effective non-Hermitian Hamiltonian $\hat{H}_{\text{eff}} = \hat{H} - i(\gamma/2) \sum_{i=1}^L \hat{L}_i^\dagger \hat{L}_i$ and by the stochastic quantum jumps determined by the jump operators \hat{L}_i [35]. While the evolution induced by \hat{H}_{eff} conserves the number of particles, the quantum jumps do not: they couple the n - and $(n-2)$ -particle sectors of the Hilbert space. For this reason, if the initial state is an eigenstate of \hat{N} , each quantum trajectory $|\psi_i(t)\rangle$ will have at any time a well-defined (although time-dependent) number of particles. We can thus label the trajectories with a double index, $|\psi_{n,\alpha}\rangle$, where n is the particle sector and α labels the trajectories belonging to the n th subspace. Note that n depends on time.

Using the fact that $\langle\psi_{n,\alpha}|\psi_{m,\beta}\rangle = 0$ for $n \neq m$, we write

$$\rho = \bigoplus_n p_n \rho_n, \quad p_n = \frac{N_n}{N_{\text{traj}}}, \quad (28)$$

where N_n is the number of trajectories belonging to the n -particle sector and

$$\rho_n = \frac{1}{N_n} \sum_{\alpha=1}^{N_n} |\psi_{n,\alpha}\rangle\langle\psi_{n,\alpha}|, \quad \text{tr}[\rho_n] = 1. \quad (29)$$

We can thus link the total purity \mathcal{P}_{tot} to the symmetry-resolved purities $\mathcal{P}(\rho_n)$, i.e., the purities of the symmetry-resolved density matrices:

$$\mathcal{P}_{\text{tot}} = \sum_n p_n^2 \mathcal{P}(\rho_n). \quad (30)$$

We now study the time evolutions of the total purity and of the symmetry-resolved purities for an initial Mott insulator

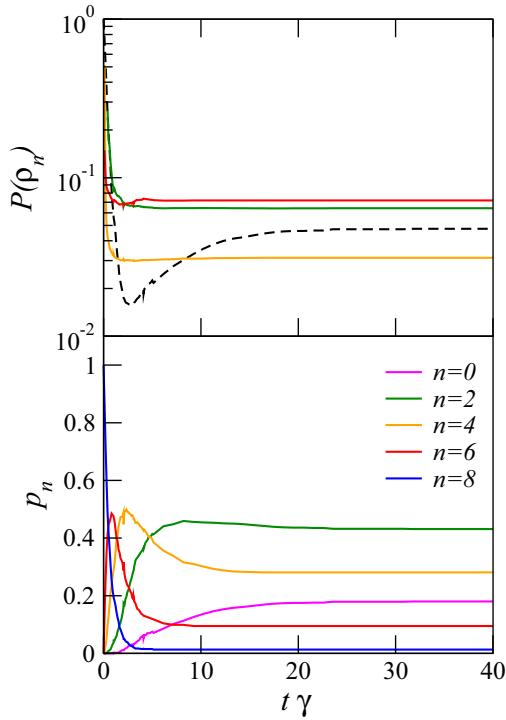


FIG. 7. Symmetry-resolved purity for the particle sectors $n = 2, 4, 6$ (solid lines) and purity of the full density matrix (dashed line). Data are obtained for a typical set of parameters, $J/\gamma = 10\hbar$, $L = 8$, and $N_{\text{traj}} = 10^3$.

with Néel order; we perform numerical simulations for $L = 8$ and $\hbar\gamma/J = 0.1$. In Fig. 7 we show the dynamics of the symmetry-resolved purities for the sectors $n = 2, 4$, and 6 (the purities for $n = 8$ and $n = 0$ are trivial and equal 1) and the behavior of the occupation probabilities p_n . The plot of \mathcal{P}_{tot} (dashed line in the top panel) shows that for $n = 2$ and 6 the symmetry-resolved purity is larger than the total one at long times, i.e., $\mathcal{P}(\rho_n) > \mathcal{P}_{\text{tot}}$.

In Fig. 8 we show the symmetry-resolved purity normalized by its minimum possible value for a given n -particle subspace, i.e., the purity of a fully mixed state $\mathcal{P}(\rho_n)_{\text{min}} = 1/\text{dim}(\mathcal{H}_n)$, where $\text{dim}(\mathcal{H}_n) = \binom{L}{n/2}^2$ is the dimension of the n -particle subspace of the Hilbert space (with $S_z = 0$). Remarkably, the asymptotic dynamics features purities which

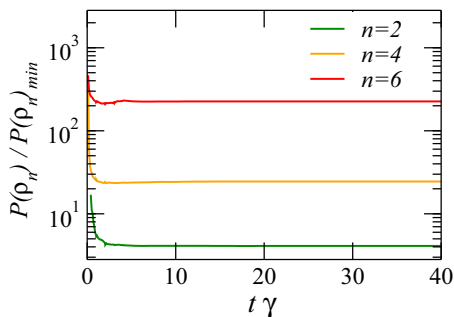


FIG. 8. Purity ratio $\mathcal{P}(\rho_n)/\mathcal{P}(\rho_n)_{\text{min}}$ for $n = 2, 4, 6$. Parameters are set as in Fig. 7.

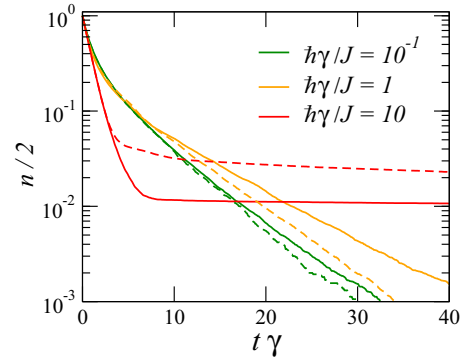


FIG. 9. Dissipative dynamics of the normalized density of a band insulator for $L = 8$ and 10^4 quantum trajectories. Different colors refer to different dissipation strengths, from $\hbar\gamma/J = 0.1$ to $\hbar\gamma/J = 10$. Solid lines: simulations with $U = \hbar\gamma$. Dashed lines: corresponding dynamics for $U = 0$. The plot highlights the collapse of the curves for $U \neq 0$ and $U = 0$ in the weakly dissipative limit.

are larger by orders of magnitude with respect to $\mathcal{P}(\rho_n)_{\text{min}}$. This is related to the fact that, although our system is subject to particle losses, the nontrivial interplay between spin conservation and dissipation leads to the creation of a nontrivial dark subspace for all possible numbers of particles n . It is interesting to observe that different from what was reported in Ref. [38], the purification process here is not transient and takes place in the long-time limit.

VII. THE EFFECT OF WEAK INTERACTIONS

We now discuss the validity of the approximation introduced in Sec. III concerning the complete neglect of the interaction term in the Hubbard Hamiltonian. The discussion presented in this article focuses on the limit of weak dissipation $\hbar\gamma \ll J$, which in most experimental situations coincides with the limit of weak interactions $U \ll J$. In Fig. 9 we show numerical simulations performed with a finite value of the interaction constant, $U = \hbar\gamma$, starting from a band insulator. The numerics clearly shows that the presence of interactions does not affect significantly the dynamics when they are weak. The curious thing is that a weak dissipation, instead, can significantly affect the dynamics.

The reason why we can safely neglect interactions but not dissipation lies in the separation of timescales between unitary hopping dynamics (very fast) and dissipative or interaction dynamics (slow). Our theoretical analysis is a perturbative treatment of dissipation, and the population equation (6) is linear in γ ; it can be regarded as a first-order expansion of the correct equation. It is well known from the standard time-dependent perturbation theory and Fermi's golden rule that a perturbative treatment of the unitary evolution due to interactions gives transition rates that are of order U^2 and thus negligible with respect to the dissipative dynamics. Since $\hbar\gamma$ and U are of the same order of magnitude, we find that interactions give a second-order correction in the weakly dissipative limit we deal with. For this reason, the whole discussion, performed in the $U = 0$ limit, is expected to provide accurate results for the weakly dissipative or interacting limit.

VIII. CONCLUSIONS

We have presented a theoretical study of the dissipative dynamics of a one-dimensional fermionic gas subject to two-body losses. Our study has focused on the nontrivial interplay between dissipation and spin conservation, as highlighted by the differential equation obeyed by the gas population [see Eq. (6)]. We have shown not only that the stationary population is due to the initial spin of the gas but also that the dynamics and its typical asymptotic decay time depend on the spin. Our analysis has focused on three kinds of initial states (Dicke states, band insulators, and several kinds of Mott insulators), characterized by different dynamical properties.

The simplicity of the proposed equations, especially when considered in the thermodynamic limit, makes us think that they could have an application in the modelization of experimental studies [28–30]. Although the experiments have so far mainly focused on the strongly dissipative Zeno limit, the fact that similar equations have been phenomenologically used for fitting experimental data [30] hints at a possible use also in this regime (after replacing γ with the Zeno decay rate). The generalization of our results to the strongly dissipative case [24] remains the most important perspective of this study. Furthermore, the possibility to stabilize Dicke states with nontrivial entanglement content opens the exciting possibility to characterize the entanglement properties of the system, analogous to what was done in Ref. [22] for bosonic particles, with possible applications to quantum metrology as well [39].

ACKNOWLEDGMENTS

We thank the Hamburg team working on Yb gases (B. Abeln, C. Becker, M. Diem, T. Petersen, and K. Sponselee) for stimulating discussions. We also acknowledge enlightening discussions with O. Giraud, F. Minganti, and B. Vermersch. This work has been partially funded by LabEx PALM (Grant No. ANR-10-LABX-0039-PALM).

APPENDIX A: DERIVATION OF EQ. (6)

We start from Eq. (4) and focus on $\langle \hat{c}_{k,\uparrow}^\dagger \hat{c}_{w,\uparrow} \hat{c}_{q,\downarrow}^\dagger \hat{c}_{z,\downarrow} \rangle_t$. We retain only the momentum-conserving ($k+q=w+z+2\pi n$) and energy-conserving ($\omega_k+\omega_q=\omega_w+\omega_z$, with $\hbar\omega_k=-2J\cos k$) correlators. We have identified five possibilities, and the first three read as follows:

(i) $k=q=w=z$. In this case,

$$\langle \hat{c}_{k,\uparrow}^\dagger \hat{c}_{w,\uparrow} \hat{c}_{q,\downarrow}^\dagger \hat{c}_{z,\downarrow} \rangle_t = \langle \hat{n}_{k,\uparrow} \hat{n}_{k,\downarrow} \rangle_t.$$

(ii) $k=w, q=z$, and $k \neq q$. In this case,

$$\langle \hat{c}_{k,\uparrow}^\dagger \hat{c}_{w,\uparrow} \hat{c}_{q,\downarrow}^\dagger \hat{c}_{z,\downarrow} \rangle_t = \langle \hat{n}_{k,\uparrow} \hat{n}_{q,\downarrow} \rangle_t, \quad k \neq q.$$

(iii) $k=z, q=w$, and $k \neq q$. In this case,

$$\langle \hat{c}_{k,\uparrow}^\dagger \hat{c}_{w,\uparrow} \hat{c}_{q,\downarrow}^\dagger \hat{c}_{z,\downarrow} \rangle_t = \langle \hat{c}_{k,\uparrow}^\dagger \hat{c}_{k,\downarrow} \hat{c}_{q,\downarrow}^\dagger \hat{c}_{q,\uparrow} \rangle_t, \quad k \neq q.$$

If we consider only these processes, we obtain

$$\langle \hat{\Pi} \rangle_t + \sum_{k \neq q} \langle \hat{n}_{k,\uparrow} \hat{n}_{q,\downarrow} \rangle_t + \langle \hat{c}_{k,\uparrow}^\dagger \hat{c}_{k,\downarrow} \hat{c}_{q,\downarrow}^\dagger \hat{c}_{q,\uparrow} \rangle_t. \quad (\text{A1})$$

We simplify this expression by introducing the explicit expressions for the spin operators. From the relations

$$\sum_k \hat{n}_{k,\uparrow,\downarrow} = \frac{\hat{N}}{2} \pm \frac{\hat{S}_z}{\hbar}, \quad \sum_k \hat{c}_{k,\uparrow}^\dagger \hat{c}_{k,\downarrow} = \frac{\hat{S}_x + i\hat{S}_y}{\hbar}, \quad (\text{A2})$$

we easily obtain

$$\frac{\hat{N}^2}{4} - \frac{\hat{S}_z^2}{\hbar^2} = \sum_{k,q} \hat{n}_{k,\uparrow} \hat{n}_{q,\downarrow}, \quad (\text{A3a})$$

$$\frac{\hat{S}_x^2 + \hat{S}_y^2 + \hbar\hat{S}_z}{\hbar^2} = \sum_{k,q} \hat{c}_{k,\uparrow}^\dagger \hat{c}_{k,\downarrow} \hat{c}_{q,\downarrow}^\dagger \hat{c}_{q,\uparrow}. \quad (\text{A3b})$$

Taking care in splitting the sums $\sum_{k,q}$ as $\sum_{k=q} + \sum_{k \neq q}$, we obtain the first five terms of Eq. (6).

We now consider the last two possibilities:

(iv) $q=\pi-k, z=\pi-w$, and $k \neq w$ and $k \neq \pi-w$. In this case,

$$\langle \hat{c}_{k,\uparrow}^\dagger \hat{c}_{w,\uparrow} \hat{c}_{q,\downarrow}^\dagger \hat{c}_{z,\downarrow} \rangle_t = \langle \hat{c}_{k,\uparrow}^\dagger \hat{c}_{w,\uparrow} \hat{c}_{\pi-k,\downarrow}^\dagger \hat{c}_{\pi-w,\downarrow} \rangle_t, \\ k \neq w, \pi-w.$$

This equation describes processes that are symmetric with respect to lattice momentum $\pi/2$, and all momenta appearing in this expression should be intended mod 2π , so that they can be restricted to the first Brillouin zone $[-\pi, \pi]$. This expression is responsible for the term $\hat{\Sigma}_{\frac{\pi}{2}}$ in Eq. (6).

(v) Finally, we have to consider umklapp processes, in which momentum is conserved mod 2π . Two classes of processes transferring momentum $+2\pi$ are possible: (i) $w=-k, z=-q$, and $k+q=\pi$ and (ii) $w=-q, z=-k$, and $k+q=\pi$. Two similar opposite processes are possible that transfer momentum -2π . These processes are responsible for the term \hat{T}_u in Eq. (6).

APPENDIX B: GAUSSIAN DENSITY MATRIX: A DYNAMICAL EQUATION FOR THE THERMODYNAMIC LIMIT

We start from Eq. (4) and focus on $\langle \hat{c}_{k,\uparrow}^\dagger \hat{c}_{w,\uparrow} \hat{c}_{q,\downarrow}^\dagger \hat{c}_{z,\downarrow} \rangle_t$. We now assume that the density matrix is Gaussian and that Wick's theorem applies:

$$\langle \hat{c}_{k,\uparrow}^\dagger \hat{c}_{w,\uparrow} \hat{c}_{q,\downarrow}^\dagger \hat{c}_{z,\downarrow} \rangle_t \sim \langle \hat{c}_{k,\uparrow}^\dagger \hat{c}_{w,\uparrow} \rangle_t \langle \hat{c}_{q,\downarrow}^\dagger \hat{c}_{z,\downarrow} \rangle_t \\ - \langle \hat{c}_{k,\uparrow}^\dagger \hat{c}_{z,\downarrow} \rangle_t \langle \hat{c}_{q,\downarrow}^\dagger \hat{c}_{w,\uparrow} \rangle_t. \quad (\text{B1})$$

Of all the correlators which appear here, we retain only those which do not have an explicit time dependence because dissipation is weak and they average to zero between two dissipative events. Thus,

$$\dot{N}(t) = -\frac{2\gamma}{L} \sum_{k,q} (\langle \hat{n}_{k,\uparrow} \rangle_t \langle \hat{n}_{q,\downarrow} \rangle_t - \langle \hat{c}_{k,\uparrow}^\dagger \hat{c}_{k,\downarrow} \rangle_t \langle \hat{c}_{q,\uparrow}^\dagger \hat{c}_{q,\downarrow} \rangle_t). \quad (\text{B2})$$

By using expressions (A2), we finally obtain the dynamical equation in (11).

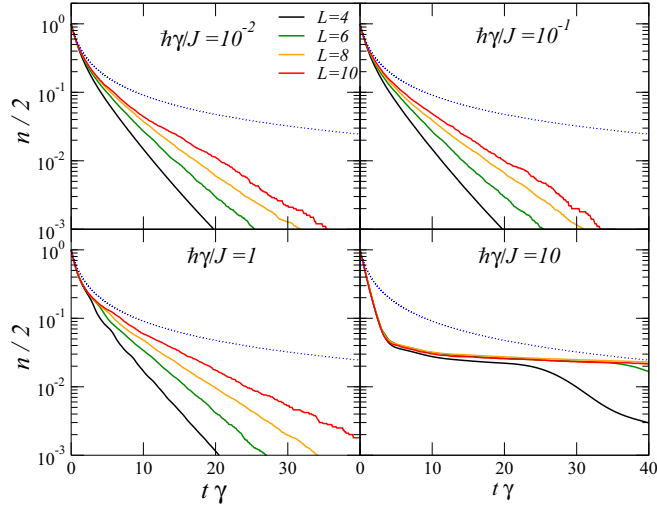


FIG. 10. Dissipative dynamics of the normalized density for a band insulator for $J/\gamma = 10^2, 10, 1$, and 0.1 . Different colors refer to different sizes, from $L = 4$ to $L = 10$. The blue dotted curve is the prediction for the thermodynamic limit in Eq. (18) and highlights the importance of finite-size effects in our simulations. The appearance of a different behavior in the strongly dissipative limit is evident.

APPENDIX C: PROOF OF RELATIONS (15) FOR DICKE STATES

In this Appendix we prove relations (15a) and (15b), which characterize Dicke states listed in Sec. IV.

Relation (15a) is simple and follows from the definition of the Dicke state: $\langle \Psi_D | \hat{S}^2 | \Psi_D \rangle = \hbar^2 \sum_N |c_N|^2 \frac{N}{2} (\frac{N}{2} + 1) = \frac{\hbar^2}{4} \langle \Psi_D | \hat{N}^2 | \Psi_D \rangle + \frac{\hbar^2}{2} \langle \Psi_D | \hat{N} | \Psi_D \rangle$.

We begin by considering the first relation in (15b). We first demonstrate it for a generic Dicke state with a well-defined number of particles N that is also an eigenstate of \hat{S}_z with eigenvalue $\hbar m$, $|D_{N,m}\rangle$. The repeated application of the spin-raising operator turns $|D_{N,m}\rangle$ into a fully polarized state: $(\hat{S}_+)^{\frac{N}{2}-m} |D_{N,m}\rangle \propto |D_{N,\frac{N}{2}}\rangle$. Since this state is fully polarized, $\hat{\Pi} |D_{N,\frac{N}{2}}\rangle = 0$. By using the expression for the spin-raising operator $\hat{S}_+ = \sum_k \hat{c}_{k\uparrow}^\dagger \hat{c}_{k\downarrow}$, it is not difficult to show that $[\hat{\Pi}, \hat{S}_+] = 0$ because $\hat{n}_{k,\uparrow} \hat{n}_{k,\downarrow} \hat{c}_{k\uparrow}^\dagger \hat{c}_{k\downarrow} = \hat{c}_{k\uparrow}^\dagger \hat{c}_{k\downarrow} \hat{n}_{k,\uparrow} \hat{n}_{k,\downarrow} = 0$. With this relation we can show that $\hat{\Pi} |D_{N,m}\rangle = 0$. From this we obtain that in general $\hat{\Pi} |D_N\rangle = 0$ and thus that $\hat{\Pi} | \Psi_D \rangle = 0$. With similar reasoning it is possible to show also the other relations in (15b) and this concludes the proof.

APPENDIX D: ADDITIONAL DATA FOR THE BAND-INSULATOR DYNAMICS

In this Appendix we present some additional data from our quantum trajectory simulations of the band-insulator dissipative dynamics. In Fig. 10 we plot the same data as in Fig. 1 at fixed $J/\hbar\gamma$ while varying L . We observe the importance of finite-size effects and the absence of any collapse at the sizes that we could consider numerically.

In Fig. 11 we plot the numerically computed $\text{Var} N_t$ and $\langle \hat{\Pi} \rangle_t$ and compare them to the expressions proposed in Eq. (19a).

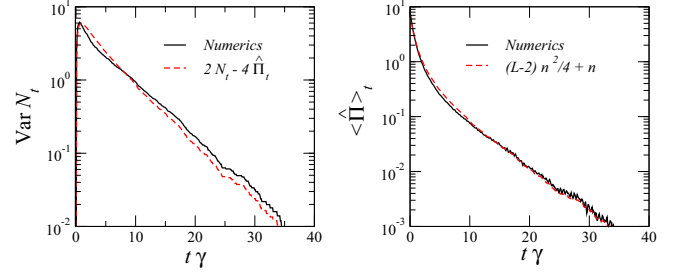


FIG. 11. $\text{Var} N_t$ (left panel) and $\langle \hat{\Pi} \rangle_t$ (right panel) for $L = 8$ and $J/\hbar\gamma = 10$. Black solid line: calculation of the two quantities using 2000 quantum trajectories. Red dashed line: approximation using formula (19a) and using the numerically computed value for $N(t)$.

APPENDIX E: ADDITIONAL DATA ON THE CALCULATION OF THE PURITY

We now comment on the convergence of the results presented in Sec. VID with respect to the number of stochastic trajectories. From Eq. (26) it is clear that the degree of accuracy in the reconstruction of the density matrix depends on N_{traj} . In particular, as N_{traj} is increased, we can account for more statistically independent realizations of the dynamics; intuitively, one expects $\mathcal{P}(\rho_n)$ to be a monotonically

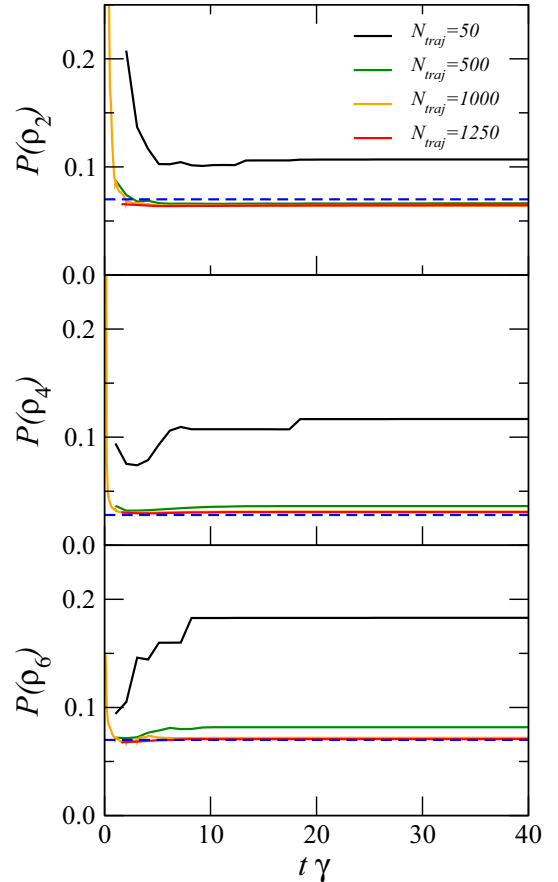


FIG. 12. Symmetry-resolved purity $\mathcal{P}(\hat{\rho}_n)$ for $n = 2, 4, 6$ for different values of N_{traj} . The blue dashed lines represent the theoretical prediction for the steady-state symmetry-resolved purity $\mathcal{P}(\rho_n) = 2/\binom{L}{n}$. Parameters are set as in Fig. 7.

decreasing function of N_{traj} . This intuition is confirmed by the numerical data presented in Fig. 12.

Decomposing the symmetry-resolved purity in terms of diagonal and off-diagonal overlaps, we get

$$\mathcal{P}(\rho_n) = \frac{1}{N_n} + \frac{1}{N_n^2} \sum_{\alpha \neq \beta}^{N_n} |\langle \psi_{n,\alpha} | \psi_{n,\beta} \rangle|^2. \quad (\text{E1})$$

Since we are interested in the $N_n \rightarrow \infty$ limit, we observe that the limiting value of the purity can be obtained by only studying the second addend on the rhs.

We now make the assumption that $N_n \propto N_{\text{traj}}$ and that $|\psi_{n,\alpha}\rangle$ are randomly distributed in the dark subspace $\mathcal{H}_n^{\text{Dark}}$, so that the off-diagonal overlaps scale as $|\langle \psi_{n,\alpha} | \psi_{n,\beta} \rangle|^2 \sim 1/\dim(\mathcal{H}_n^{\text{Dark}})$ for $\alpha \neq \beta$. In the limit $N_n \rightarrow \infty$ we obtain

$$\mathcal{P}(\rho_n) \simeq \frac{1}{\dim(\mathcal{H}_n^{\text{Dark}})}. \quad (\text{E2})$$

In our specific case, we can estimate the dimension of the dark subspace by counting the number of antisymmetric or-

bit wave functions associated with the fully symmetric spin part of the wave function, a Dicke state with $S = n/2$ and $S_z = 0$. Thus, $\dim(\mathcal{H}_n^{\text{Dark}}) = \binom{L}{n}$. Equation (E2) provides a very good estimation of the asymptotic value of the symmetry-resolved purity, as shown in Fig. 12, where the convergence with N_{traj} is also shown.

By numerical inspection, the asymptotic purity value is $\mathcal{P}(\rho_n) = 2/\binom{L}{n}$; we do not understand the reason for the factor of 2 appearing in the formula, which points to a lack of ergodicity and to the fact that the only half of the dark subspace is explored by the dynamics. We pose that this is due to the specific spin structure of the initial Néel state and that a Mott insulator with randomly oriented spins would explore the full dark state; we leave a more systematic study to the future.

Finally, we stress that this numerical computation is quite heavy in terms of memory since it requires us to allocate N_{traj} wave functions of the many-body system for many values of t , which limits our analysis to $N_{\text{traj}} = 1250$.

-
- [1] T. Langen, R. Geiger, and J. Schmiedmayer, Ultracold atoms out of equilibrium, *Annu. Rev. Condens. Matter Phys.* **6**, 201 (2015).
- [2] W. H. Zurek, Decoherence, einselection, and the quantum origins of the classical, *Rev. Mod. Phys.* **75**, 715 (2003).
- [3] B. Laburthe Tolra, K. M. O'Hara, J. H. Huckans, W. D. Phillips, S. L. Rolston, and J. V. Porto, Observation of Reduced Three-Body Recombination in a Correlated 1D Degenerate Bose Gas, *Phys. Rev. Lett.* **92**, 190401 (2004).
- [4] T. Kraemer, M. Mark, P. Waldburger, J. G. Danzl, C. Chin, B. Engeser, A. D. Lange, K. Pilch, A. Jaakkola, H.-C. Nägerl, and R. Grimm, Evidence for Efimov quantum states in an ultracold gas of caesium atoms, *Nature (London)* **440**, 315 (2006).
- [5] S. E. Pollack, D. Dries, and R. G. Hulet, Universality in three- and four-body bound states of ultracold atoms, *Science* **326**, 1683 (2009).
- [6] S. K. Baur and E. J. Mueller, Two-body recombination in a quantum-mechanical lattice gas: Entropy generation and probing of short-range magnetic correlations, *Phys. Rev. A* **82**, 023626 (2010).
- [7] P. Grišins, B. Rauer, T. Langen, J. Schmiedmayer, and I. E. Mazets, Degenerate Bose gases with uniform loss, *Phys. Rev. A* **93**, 033634 (2016).
- [8] I. Bouchoule, M. Schemmer, and C. Henkel, Cooling phonon modes of a Bose condensate with uniform few body losses, *SciPost Phys.* **5**, 043 (2018).
- [9] M. Schemmer and I. Bouchoule, Cooling a Bose Gas by Three-Body Losses, *Phys. Rev. Lett.* **121**, 200401 (2018).
- [10] L. H. Dogra, J. A. P. Glidden, T. A. Hilker, C. Eigen, E. A. Cornell, R. P. Smith, and Z. Hadzibabic, Can Three-Body Recombination Purify a Quantum Gas?, *Phys. Rev. Lett.* **123**, 020405 (2019).
- [11] N. Syassen, D. M. Bauer, M. Lettner, T. Volz, D. Dietze, J. J. García-Ripoll, J. I. Cirac, G. Rempe, and S. Dürr, Strong dissipation inhibits losses and induces correlations in cold molecular gases, *Science* **320**, 1329 (2008).
- [12] J. J. García-Ripoll, S. Dürr, N. Syassen, D. M. Bauer, M. Lettner, G. Rempe, and J. I. Cirac, Dissipation-induced hardcore boson gas in an optical lattice, *New J. Phys.* **11**, 013053 (2009).
- [13] A. Kantian, M. Dalmonte, S. Diehl, W. Hofstetter, P. Zoller, and A. J. Daley, Atomic Color Superfluid via Three-Body Loss, *Phys. Rev. Lett.* **103**, 240401 (2009).
- [14] A. J. Daley, J. M. Taylor, S. Diehl, M. Baranov, and P. Zoller, Atomic Three-Body Loss as a Dynamical Three-Body Interaction, *Phys. Rev. Lett.* **102**, 040402 (2009).
- [15] M. Roncaglia, M. Rizzi, and J. I. Cirac, Pfaffian State Generation by Strong Three-Body Dissipation, *Phys. Rev. Lett.* **104**, 096803 (2010).
- [16] A. Beige, D. Braun, B. Tregenna, and P. L. Knight, Quantum Computing Using Dissipation to Remain in a Decoherence-Free Subspace, *Phys. Rev. Lett.* **85**, 1762 (2000).
- [17] S. Diehl, A. Micheli, A. Kantian, B. Kraus, H.-P. Büchler, and P. Zoller, Quantum states and phases in driven open quantum systems with cold atoms, *Nat. Phys.* **4**, 878 (2008).
- [18] F. Verstraete, M. M. Wolf, and J. I. Cirac, Quantum computation, quantum state engineering, and quantum phase transitions driven by dissipation, *Nat. Phys.* **5**, 633 (2009).
- [19] S. Diehl, E. Rico, M. A. Baranov, and P. Zoller, Topology by dissipation in atomic quantum wires, *Nat. Phys.* **7**, 971 (2011).
- [20] F. Iemini, D. Rossini, R. Fazio, S. Diehl, and L. Mazza, Dissipative topological superconductors in number-conserving systems, *Phys. Rev. B* **93**, 115113 (2016).
- [21] G. Kordas, D. Witthaut, P. Buonsante, A. Vezzani, R. Burioni, A. I. Karanikas, and S. Wimberger, The dissipative Bose-Hubbard model, *Eur. Phys. J.: Spec. Top.* **224**, 2127 (2015).
- [22] S. Goto and I. Danshita, Measurement-induced transitions of the entanglement scaling law in ultracold gases with controllable dissipation, *Phys. Rev. A* **102**, 033316 (2020).
- [23] I. Bouchoule, B. Doyon, and J. Dubail, The effect of atom losses on the distribution of rapidities in the one-dimensional Bose gas, *SciPost Phys.* **9**, 44 (2020).

- [24] D. Rossini, A. Ghermaoui, M. B. Aguilera, R. Vatré, R. Bouganne, J. Beugnon, F. Gerbier, and L. Mazza, Strong correlations in lossy one-dimensional quantum gases: From the quantum Zeno effect to the generalized Gibbs ensemble, *Phys. Rev. A* **103**, L060201 (2021).
- [25] I. Bouchoule and J. Dubail, Breakdown of Tan's Relation in Lossy One-Dimensional Bose Gases, *Phys. Rev. Lett.* **126**, 160603 (2021).
- [26] M. Nakagawa, N. Kawakami, and M. Ueda, Exact Liouvillian Spectrum of a One-Dimensional Dissipative Hubbard Model, *Phys. Rev. Lett.* **126**, 110404 (2021).
- [27] M. Foss-Feig, A. J. Daley, J. K. Thompson, and A. M. Rey, Steady-State Many-Body Entanglement of Hot Reactive Fermions, *Phys. Rev. Lett.* **109**, 230501 (2012).
- [28] B. Yan, S. A. Moses, B. Gadway, J. Covey, K. R. A. Hazzard, A. M. Rey, D. S. Jin, and J. Ye, Observation of dipolar spin-exchange interactions with lattice-confined polar molecules, *Nature (London)* **501**, 521 (2013).
- [29] B. Zhu, B. Gadway, M. Foss-Feig, J. Schachenmayer, M. L. Wall, K. R. A. Hazzard, B. Yan, S. A. Moses, J. P. Covey, D. S. Jin, J. Ye, M. Holland, and A. M. Rey, Suppressing the Loss of Ultracold Molecules via the Continuous Quantum Zeno Effect, *Phys. Rev. Lett.* **112**, 070404 (2014).
- [30] K. Sponselee, L. Freystatzky, B. Abeln, M. Diem, B. Hundt, A. Kochanke, T. Ponath, B. Santra, L. Mathey, K. Sengstock, and C. Becker, Dynamics of ultracold quantum gases in the dissipative Fermi-Hubbard model, *Quantum Sci. Technol.* **4**, 014002 (2019).
- [31] M. Nakagawa, N. Tsuji, N. Kawakami, and M. Ueda, Dynamical Sign Reversal of Magnetic Correlations in Dissipative Hubbard Models, *Phys. Rev. Lett.* **124**, 147203 (2020).
- [32] T. Tomita, S. Nakajima, I. Danshita, Y. Takasu, and Y. Takahashi, Observation of the Mott insulator to superfluid crossover of a driven-dissipative Bose-Hubbard system, *Sci. Adv.* **3**, e1701513 (2017).
- [33] F. Lange, Z. Lenarčič, and A. Rosch, Time-dependent generalized Gibbs ensembles in open quantum systems, *Phys. Rev. B* **97**, 165138 (2018).
- [34] K. Mallayya, M. Rigol, and W. De Roeck, Prethermalization and Thermalization in Isolated Quantum Systems, *Phys. Rev. X* **9**, 021027 (2019).
- [35] A. J. Daley, Quantum trajectories and open many-body quantum systems, *Adv. Phys.* **63**, 77 (2014).
- [36] J. Johansson, P. Nation, and F. Nori, Qutip: An open-source Python framework for the dynamics of open quantum systems, *Comput. Phys. Commun.* **183**, 1760 (2012).
- [37] J. Johansson, P. Nation, and F. Nori, Qutip 2: A Python framework for the dynamics of open quantum systems, *Comput. Phys. Commun.* **184**, 1234 (2013).
- [38] V. Vitale, A. Elben, R. Kueng, A. Neven, J. Carrasco, B. Kraus, P. Zoller, P. Calabrese, B. Vermersch, and M. Dalmonte, Symmetry-resolved dynamical purification in synthetic quantum matter, [arXiv:2101.07814](https://arxiv.org/abs/2101.07814).
- [39] I. Apellaniz, B. Lücke, J. Peise, C. Klempt, and G. Tóth, Detecting metrologically useful entanglement in the vicinity of Dicke states, *New J. Phys.* **17**, 083027 (2015).